Electronic structure of Mn$_{12}$ derivatives on the clean and functionalized Au surface

S. Voss,* M. Fonin, and U. Rüdiger

Fachbereich Physik, Universität Konstanz, 78457 Konstanz, Germany

M. Burgert and U. Groth

Fachbereich Chemie, Universität Konstanz, 78457 Konstanz, Germany

Yu. S. Dedkov

Institut für Festkörperphysik, Technische Universität Dresden, 01062 Dresden, Germany
(Received 1 September 2006; revised manuscript received 18 October 2006; published 3 January 2007)

We present a detailed study on the electronic properties of monolayers of Mn$_{12}$ derivatives chemically grafted on clean as well as on functionalized Au(111) surfaces. Scanning tunneling microscopy and x-ray photoelectron spectroscopy were employed to ensure the successful monolayer deposition. Unoccupied and occupied valence band states in the electronic structure of Mn$_{12}$-clusters were probed by means of x-ray absorption spectroscopy (XAS) and resonant photoelectron spectroscopy (RPES) at the Mn $2p$-$3d$ absorption edge, respectively. XAS measurements reveal a significant difference between the Mn oxidation states of Mn$_{12}$ cores bound to the Au surface compared with the single crystal environment. Direct deposition of Mn$_{12}$ derivatives onto the Au surface leads to a strong fragmentation of Mn$_{12}$ cores. An appropriate combination of Mn$_{12}$ cluster and substrate functionalization leads to formation of Mn$_{12}$ monolayers with a large fraction of Mn$_{12}$ cores retaining their structural integrity upon surface deposition. By extracting the Mn $3d$ partial density of states from the RPES spectra a very good agreement with previously reported LDA+U calculations on Mn$_{12}$ for U=4 eV [Boukhvalov *et al.*, J. Electron Spectrosc. Relat. Phenom. **137–140**, 735 (2004)] was found, showing the importance of electron correlation effects in Mn$_{12}$ systems.

PACS number(s): 75.50.Xx, 79.60.−i, 78.70.Dm

I. INTRODUCTION

In recent years, single molecule magnets (SMMs) have attracted much attention due to their unique properties such as quantum tunneling of magnetization (QTM) and hysteresis of pure molecular origin,[1] making these materials potential candidates for future applications in ultradensity data storage devices or quantum computing.[2] The most widely investigated class of SMMs is the Mn$_{12}$ group, comprised of Mn$_{12}$-acetate, the first SMM discovered,[1] and its derivatives. The Mn$_{12}$ core consists of four Mn^{4+} (S=3/2) ions surrounded by an antiferromagnetically coupled ring of eight Mn^{3+} (S=2) ions,[3] resulting in a ground state spin S=10.[4] The high spin ground state, combined with large uniaxial magnetic anisotropy, results in an energy barrier for spin reversal, giving rise to superparamagnetic behavior at low temperature.[1] In the range of 2 K the magnetization relaxation becomes extremely slow, and each molecule behaves like a classical magnet with a magnetic moment of $20\mu_B$. The observation of stepwise magnetization hysteresis loops below the blocking temperature can be attributed to isolated molecules showing QTM rather than to long-range interactions. Up to date, experiments on magnetic properties of Mn$_{12}$, revealing stepwise magnetization hysteresis, have been performed exclusively on bulklike material[5–7] while the magnetic as well as the electronic properties of the individual molecules or SMM monolayers on a surface remain to large extent unknown. The first approach to the investigation of the fundamental physical properties of Mn$_{12}$ derivatives are transport measurements in a kind of molecular electronics setup where the individual molecules are placed between two nanometer-sized electrical contacts. Very recently, two groups reported such transport measurements through Mn$_{12}$ clusters in a single-molecule transistor geometry where signatures of molecular magnetism were found.[8,9] On the other hand, scanning tunneling microscopy (STM) and spectroscopy (STS) can be implemented to investigate the electronic and magnetic states of Mn$_{12}$ molecules while the preparation of individual Mn$_{12}$ clusters or SMM monolayers on surfaces remains the most crucial issue. Recently, many different approaches to this goal have been reported with the most promising grafting techniques based on direct deposition either via thiol modified ligands of Mn$_{12}$ interacting with the Au(111) surface[10–12] or taking advantage of electrostatic interactions.[13] Additionally, bonding of SMMs to functionalized Au(111) (Ref. 7) or Si(100) (Refs. 14 and 15) surfaces via a ligand-exchange reaction was implemented. In these experiments, scanning probe techniques revealed the presence of Mn$_{12}$ clusters on the surface while x-ray photoelectron spectroscopy (XPS) yielded a significant manganese peak after deposition of Mn$_{12}$ clusters on surfaces. Nevertheless, no magnetization hysteresis could be observed for monolayers of Mn$_{12}$ SMMs although high quality scanning tunneling microscopy images of ordered monolayers were obtained.[7] Moreover, detailed investigations of electronic properties of monolayers on surfaces are still lacking. Only very recently, Pennino *et al.*[16] reported an x-ray absorption spectroscopy (XAS) and valence band resonant photoelectron spectroscopy (RPES) study of the Mn$_{12}$ derivative {Mn$_{12}$O$_{12}$[O$_2$C(CH$_2$)$_{15}$SAc]$_{16}$} grafted on Au(111), stating that surface deposition of SMMs does not significantly affect the cluster integrity. However, the XAS line shape and the Mn $3d$ partial density of states (PDOS) extracted from RPES
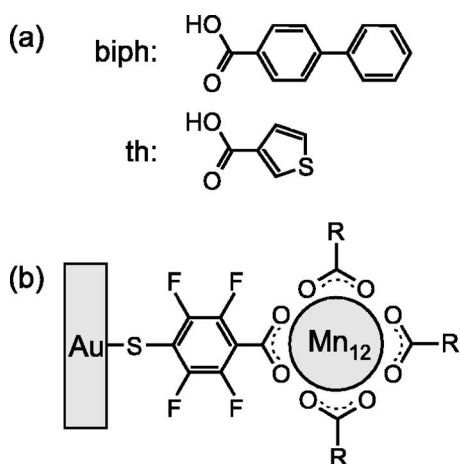
FIG. 1. In (a) the ligands of Mn_{12}-biph and Mn_{12}-th are shown. (b) Schematic representation of the Mn_{12} molecule chemically bound to the Au(111) surface via ligand exchange reaction with 4-MTBA.

showed some discrepancies compared with the XAS of a SMM single crystal and with LDA+U calculations, respectively.

In this paper, we present the results of a combined STM, XPS, XAS, and RPES study of two Mn_{12} derivatives chemically grafted on the Au(111) surface. Different preparation techniques were used for the preparation of SMM monolayers: direct deposition of Mn_{12} derivatives with thiol-modified ligands as well as grafting of SMMs on a functionalized surface via ligand exchange reaction. STM and XPS measurements performed on the SMM monolayers on Au(111) reveal that direct deposition of SMMs on Au(111) leads to fragmentation of the Mn_{12} derivative molecules while appropriate functionalization of the surface followed by SMM deposition via ligand exchange reaction is found to be suitable to deposit intact SMMs on the Au surface. The electronic properties of the SMM monolayers prepared by the latter technique have been studied in detail and compared with band structure calculations.

II. EXPERIMENTAL

Single crystals of Mn_{12}-thiophene-3-carboxylate $[Mn_{12}O_{12}(O_2CC_4H_3S)_{16}(H_2O)_4]$ (Mn_{12}-th) and Mn_{12}-biphenyl-carboxylate $[Mn_{12}O_{12}(O_2CC_6H_4C_6H_5)_{16}(H_2O)_4]$ (Mn_{12}-biph) with average dimensions of $1 \times 1 \times 0.5$ mm^3 were prepared according to the procedures reported by Lim *et al.*[17] and Ruiz-Molina *et al.*,[18] respectively. The ligands of Mn_{12}-biph and Mn_{12}-th are shown in Fig. 1(a). SMM monolayers were prepared by immersion of (111)-oriented Au films on silicon wafers with Ti adhesion layer[19] (for XAS, RPES) or of an Au(111) single crystal (STM, XPS) into the SMM solution. Comparability of experiments realized on Au(111) single crystals with those realized on Au(111) films on silicon wafers was guaranteed by comparative UPS and XPS measurements as well as STM measurements on Mn_{12} monolayers deposited on strongly Ar$^+$-sputtered Au(111) single crystal surfaces. 0.04 mM solution of Mn_{12}-th in

dichloromethane (DCM) was used for direct deposition (10 min) via physisorption due to the strong S-Au interaction. 2 mM 4-Mercapto-2,3,5,6-tetrafluorobenzoic acid (4-MTBA) solution in ethanol (5 min) was used for functionalization of the Au surface. 0.04 mM solution of Mn_{12}-th and 0.03 mM solution of Mn_{12}-biph in DCM was used for monolayer deposition (2 h) using the ligand exchange reaction described by Artus *et al.*[20] A schematic representation of the Mn_{12} molecule chemically bound to the Au(111) surface via ligand exchange reaction with 4-MTBA is shown in Fig. 1(b). All samples were thoroughly rinsed with the respective solvent after preparation and dried in a stream of dry nitrogen. The samples were introduced into the ultrahigh vacuum (UHV) chambers via ultra-fast load locks to avoid surface contaminations.

STM and XPS measurements were performed with an Omicron Multiprobe UHV system (base pressure 10^{-11} mbar) at room temperature. In all STM experiments performed with the Omicron VT AFM/STM electrochemically etched tungsten tips, flashed by electron bombardment were used. XPS spectra were collected using the nonmonochromatized Al K_α line (1486.6 eV). The energy resolution of the Omicron EA 125 analyzer was set to 0.65 eV full width at half maximum (FWHM).

XAS and RPES measurements were performed at BESSY (Berlin) using radiation from the RGBL-PGM ultrahigh energy-resolution dipole beamline. The base pressure was below 8×10^{-10} mbar. XAS spectra were taken at room temperature with a photon-energy resolution of 80 meV FWHM in total electron yield mode. The RPES spectra were recorded with a CLAM 4 energy analyzer with energy resolution set to 150 meV FWHM. Mn(II)oxide (99.999%, Aldrich), Mn(III)oxide (99.999%, Aldrich), and Mn(IV)oxide (99.99%, Aldrich) were used as reference compounds in XAS experiments.

III. RESULTS AND DISCUSSION

In order to confirm the formation of SMM monolayers, STM and XPS measurements were performed. Figure 2 shows STM images of (a) the Au(111) surface functionalized with 4-MTBA, (b) Mn_{12}-biph deposited on the Au(111) surface functionalized with 4-MTBA, (c) Mn_{12}-th deposited on the Au(111) surface functionalized with 4-MTBA, and (d) Mn_{12}-th after direct deposition on Au(111). In Fig. 2(a) the characteristic steps of the Au(111) surface are still visible after deposition of 4-MTBA. Typical depressions as usually observed in monolayers of aromatic thiols[21] are present confirming the successful deposition. The image shows the absence of contaminations on the functionalized surface, ensuring that any additional component deposited in the further preparation process can be clearly identified. Figure 2(b) shows the 4-MTBA functionalized Au(111) surface after deposition of Mn_{12}-biph. The image was smoothed to compensate for spiking induced by tip contaminations. Isolated round-shaped clusters are clearly visible in front of a diffuse background. The average lateral size of the clusters was measured to be (6.6 ± 0.9) nm FWHM which is somewhat larger than the expected Mn_{12}-biph diameter of about 3 nm. The

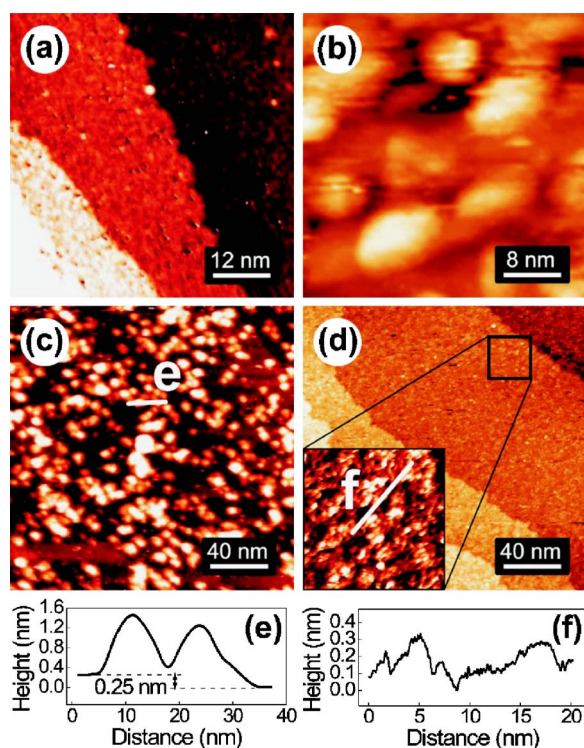FIG. 2. (Color online) (a) 60×60 nm^2 STM image of 4-MTBA on Au(111). (b) 40×40 nm^2 STM image of Mn$_{12}$-biph on Au(111) functionalized with 4-MTBA. (c) 200×200 nm^2 STM image of Mn$_{12}$-th on Au(111) with 4-MTBA. (d) 200×200 nm^2 STM image of Mn$_{12}$-th directly deposited on Au(111). The inset (30×30 nm^2) shows a dense layer of molecular fragments. (e) Height profile along the line sketched in (c). (f) Height profile along the line sketched in (d). Scanning parameters for all images $U_T = +1$ V, $I_T = 5-7$ pA.

discrepancy between the measured and expected diameter can be attributed to the finite STM tip radius. The average cluster height was measured to be (1.3 ± 0.3) nm (expected height ~ 2.2 nm) with the accuracy of the measurements limited by the high background corrugation.

For Mn$_{12}$-th deposited on the 4-MTBA-functionalized Au(111) surface [Fig. 2(c)], a sub-monolayer of nearly identical clusters was observed. The cluster height of (1.1 ± 0.2) nm is close to the expected height of Mn$_{12}$-th molecules of 1.4 nm. The average cluster diameter is (5.4 ± 0.6) nm FWHM (expected diameter ~ 2 nm) while the deviation from the expected value is again explained by the finite tip curvature. The characteristic steps of Au(111) are still visible in image (c) [see also height profile (e)], indicating the deposition of a submonolayer of Mn$_{12}$-th. The observed clusters retained their positions upon scanning confirming the chemical bonding to the Au(111) surface.

In the case of Mn$_{12}$-th directly deposited onto Au(111) [Fig. 2(d)] a relatively flat layer of small clusters with an average corrugation below 3 Å [Fig. 2(f)] was observed. The Au(111) steps are clearly visible after the Mn$_{12}$ deposition. The inset in Fig. 2(d) shows small clusters, indicating a fragmentation of Mn$_{12}$-th. The scanning conditions were highly stable, indicating a strong interaction between clusters and Au substrate. The STM images of Mn$_{12}$-th directly deposited
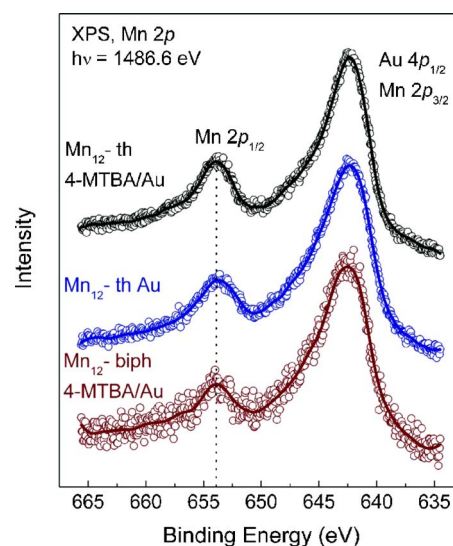

FIG. 3. (Color online) Mn $2p$ core level spectra ($h\nu = 1486.6$ eV) of Mn$_{12}$-th on 4-MTBA/Au, Mn$_{12}$-th directly deposited on Au, and Mn$_{12}$-biph on 4-MTBA/Au. Open circles represent experimental data while solid lines were obtained by fast Fourier transformation (FFT) averaging.

onto Au(111) show no agreement with previously reported AFM (Ref. 22) and STM (Ref. 23) investigations where layers of large clusters were observed. This discrepancy could be possibly due to the difference in the preparation technique, in particular difference in the solvents used for the monolayer deposition. In the case of AFM measurements the difference can be also due to the limited resolution of previous AFM measurements compared with the present STM measurements.

The images of Mn$_{12}$-th and Mn$_{12}$-biph deposited on functionalized Au(111) indicate a successful ligand exchange reaction. The difference of 1.2 nm between the measured diameters of Mn$_{12}$-th [(5.4 ± 0.6) nm] and Mn$_{12}$-biph [(6.6 ± 0.9) nm] on 4-MTBA agrees with the difference of 1 nm between the expected diameters of 2 and 3 nm, respectively, while the deviation of measured values from those expected is probably due to the finite STM tip radius becoming relevant when imaging highly corrugated surfaces. However, direct deposition of Mn$_{12}$-th onto Au(111) leads to fragmentation due to the strong S-Au interaction. A possible explanation for this effect will be given below.

Figure 3 shows XPS spectra of Mn$_{12}$-th and Mn$_{12}$-biph monolayers on Au(111) and on 4-MTBA functionalized Au(111), respectively. The Mn $2p_{1/2}$-peak position (653.9 eV) is identical for all three samples within experimental resolution and is in agreement with previously reported spectra.[12,13,24,25] The nearly identical intensities support the idea of monolayer formation. However, comparison of the spectra with the corresponding STM images illustrates that the presence of a Mn $2p$ peak cannot corroborate the existence of intact Mn$_{12}$ clusters in case of Mn$_{12}$-th. Moreover, XPS and STM measurements are insufficient for the determination of the chemical integrity of Mn$_{12}$ clusters deposited onto the Au surface. To this end, XAS measurements can be used for investigation of the nature of Mn$_{12}$ clusters deposited on surfaces.
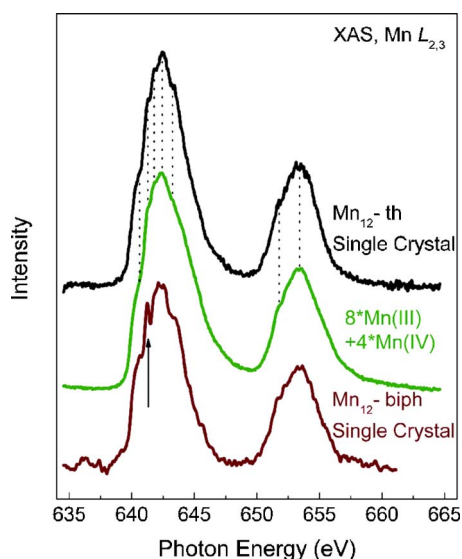
FIG. 4. (Color online) XAS spectra obtained from Mn_{12}-th and Mn_{12}-biph single crystals compared to the sum of the Mn^{3+} and Mn^{4+} contributions (see Fig. 5) weighted by their relative abundance in the molecule.
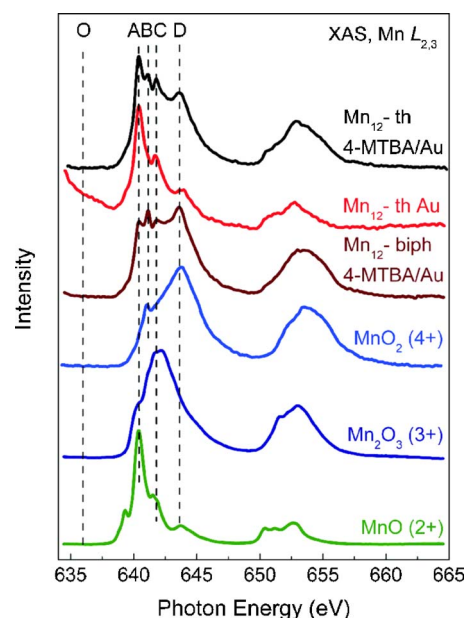

FIG. 5. (Color online) XAS spectra obtained from Mn_{12}-th and Mn_{12}-biph monolayers compared to reference absorption spectra of MnO, Mn_2O_3, and MnO_2.

In contrast to nowadays mostly employed undulator beam lines, which deliver an extremely high photon flux in the form of a discrete spectrum, the RGBL-PGM beam line provides low-intensity radiation continuously distributed in a wide range (30 to 1500 eV) and is thus suitable for spectroscopic studies of molecular samples. XAS spectra recorded within 2 h of exposure of the sample to synchrotron radiation were compared to each other, showing no difference in the line shape due to a possible photon induced damage, supporting the suitability of the RGBL-PGM beam line for experiments on Mn_{12} clusters. Figure 4 shows XAS Mn $L_{2,3}$ spectra of Mn_{12}-th and Mn_{12}-biph single crystals. The spectrum of Mn_{12}-biph shows a complex multiplet structure which is in agreement with previous measurements on Mn_{12} single crystals.[26,27] However, the absorption spectrum of Mn_{12}-th shows a slightly different line shape compared with Mn_{12}-biph. For example, the feature around 641.2 eV clearly visible in the Mn_{12}-biph spectrum (black arrow in Fig. 4) is missing in the spectrum of Mn_{12}-th. The absence of the feature around 641.2 eV in the Mn_{12}-th spectrum might be assigned either to another crystal symmetry of Mn_{12}-th and Mn_{12}-biph or to deviations in the single crystal quality. The Mn_{12}-th single crystals used for this experiment were of excellent quality (perfectly shaped, extremely robust, few solvent residuals) while the Mn_{12}-biph single crystals seemed to contain a slightly larger amount of solvent residuals, which is commonly observed for Mn_{12} crystals. The XAS spectra can be perfectly fitted by the sum of the Mn^{3+} (Mn_2O_3) and Mn^{4+} (MnO_2) contributions (see Fig. 5) weighted by their relative abundance in the molecule except for the feature around 641.2 eV in the case of Mn_{12}-biph.

Figure 5 shows a comparison of XAS Mn $L_{2,3}$ spectra obtained from Mn_{12}-th on the Au surface (clean as well as functionalized with 4-MTBA) and Mn_{12}-biph on the Au surface functionalized with 4-MTBA. The reference absorption spectra of MnO (Mn^{2+}), Mn_2O_3 (Mn^{3+}), and MnO_2 (Mn^{4+}) are also presented for comparison. The presented absorption spectra reveal different line shapes which deviate from the corresponding XAS spectra line shape obtained from the single crystals. The comparison of the main spectral features of the SMM monolayers (labeled *A*, *B*, *C*, and *D* in Fig. 5) to the reference spectra shows that, in contrast to solely Mn^{3+} and Mn^{4+} contributions to the single crystal XAS spectra (Fig. 4), a significant Mn^{2+} contribution is visible in the case of SMM monolayers (label *A*), suggesting a partial reduction of the Mn_{12} core after deposition on the Au surface. Especially, in the case of Mn_{12}-th deposited directly on the clean Au surface the Mn^{2+} contribution is very strong with the spectral line shape nearly identical to those of MnO (Mn^{2+}), suggesting a complete reduction of the Mn_{12} core. As for Mn_{12}-biph and Mn_{12}-th on 4-MTBA/Au the strong contributions from Mn^{3+} (*C*) and Mn^{4+} (*D*) indicate that a large fraction of intact molecules was deposited on the Au surface. The absorption spectrum of Mn_{12}-biph on 4-MTBA/Au exhibiting a four-peak structure differs slightly from those of Mn_{12}-th on 4-MTBA/Au by a smaller Mn^{2+} contribution.

The XAS measurements are consistent with the STM observations, suggesting a fragmentation of the Mn_{12} core after direct deposition onto Au(111). The decomposition of the Mn_{12} core can be attributed to the in-solvent ligand diffusion during chemical preparation in combination with a strong ligand interaction with the Au surface. The strong S-Au interaction leads to a bonding of free ligands in the vicinity of surface-bound Mn_{12} clusters to the Au surface. Upon solvent evaporation those Mn_{12} clusters with incomplete ligand configuration are reduced by absorption of substrate electrons while the stabilizing solvent matrix is missing. This effect induces a complete destruction of Mn_{12}-th deposited on a clean Au surface. In the case of 4-MTBA covered Au the effect seems to be screened to a large extent. In the case of Mn_{12}-biph a large number of stable Mn_{12}-cores is present on
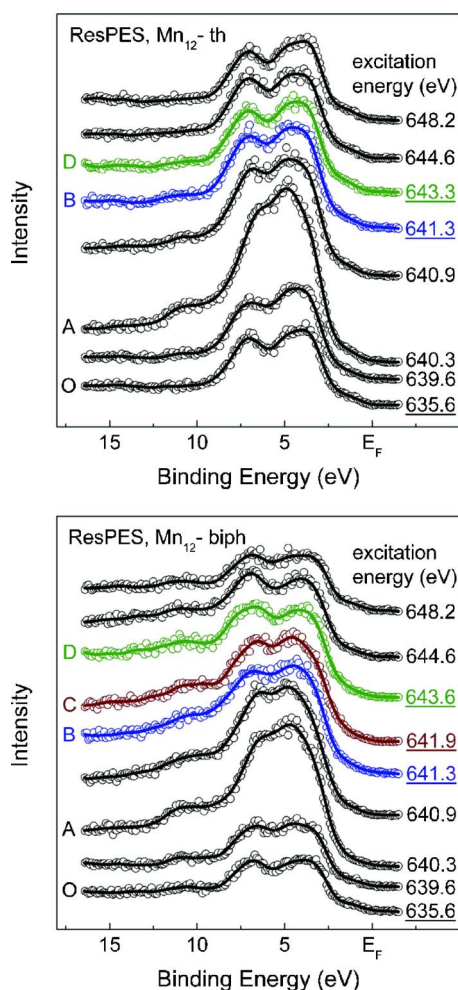
FIG. 6. (Color online) Valence band photoemission spectra of Mn$_{12}$-th (upper panel) and Mn$_{12}$-biph (lower panel) on 4-MTBA/Au measured at the Mn $2p$ absorption edge at photon energies marked in the image. The spectra used for extraction of the Mn $3d$ PDOS are underlined and marked by O, B, D (Mn$_{12}$-th) and O, B, C, D (Mn$_{12}$-biph), respectively. Open circles represent experimental data while solid lines were obtained by FFT averaging.

the surface while in the case of Mn$_{12}$-th a driving force to a higher Mn^{2+} fraction is imposed by defects in the 4-MTBA layer allowing some thiophene ligands to interact with Au atoms via S-Au interactions and thus leading to a higher fragmentation ratio.

No further measurements on Mn$_{12}$-th deposited directly on Au were performed since there is no significant Mn^{3+} or Mn^{4+} contribution to the XAS spectrum. Due to the presence of distinct Mn^{3+} and Mn^{4+} signals in the XAS spectra in Fig. 5 we measured RPES spectra of Mn$_{12}$-th and Mn$_{12}$-biph on 4-MTBA functionalized Au surfaces. The Mn L_3 absorption edge is superimposed by the Au N_2 absorption edge. However, due to the complete filling of the Au $5d$ shell and only a slight hybridization with the $6p$-s states[29] the Au N_2 contribution from the Au substrate to the RPES valence band spectra is insignificant.[16]

Figure 6 shows the valence band spectra of Mn$_{12}$-th (upper panel) and Mn$_{12}$-biph (lower panel) monolayers on 4-MTBA/Au measured by tuning the photon energy over the
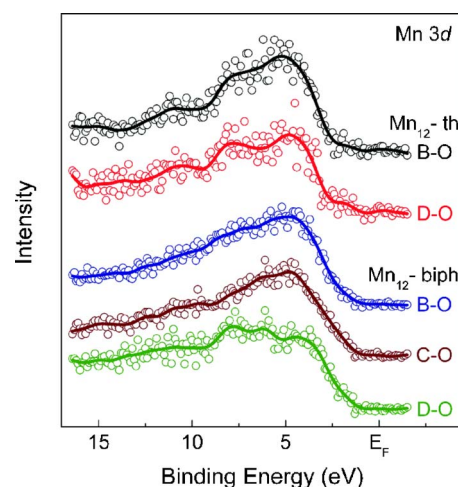

FIG. 7. (Color online) Mn $3d$ PDOS of Mn$_{12}$-th and Mn$_{12}$-biph obtained by subtraction of the off-resonance spectra from the on-resonance ones labeled in Fig. 6. The PDOS is spread uniformly over a range of about 10 eV while a band gap sets in 1 eV below the Fermi level. The *D-O* spectra are in good agreement with LDA+U calculations for $U=4$ eV [Mn$_{12}$-th: (Ref. 28), Mn$_{12}$-biph: (Ref. 16)]. Open circles represent experimental data while solid lines were obtained by FFT averaging.

$2p \rightarrow 3d$ excitation threshold. Three distinct peaks are visible around about 4, 7, and 11 eV, respectively. The peaks around 4 and 7 eV in the off-resonance spectra can be mainly attributed to Au $5d$ valence states from the substrate. A small shoulder in the region $0-2$ eV of binding energy can also be attributed to the Au substrate as no resonant enhancement was observed here. The off-resonance spectra obtained at 635.6 eV photon energy are labeled as O while the on-resonance spectra between 639.6 and 644.6 eV show a typical resonant behavior which gives rise to a change of the spectral line shape as well as another peak emerging around 11 eV which can be assigned to the Mn $3d$ contribution. The observations are in agreement with recently published RPES spectra obtained from monolayers of the single molecule magnet [Mn$_{12}$O$_{12}$(O$_2$C(CH$_2$)$_{15}$SAc)$_{16}$].[16] The strongest on-resonance spectrum at 640.3 eV is mainly attributed to a Mn^{2+} contribution and is thus not suited for further investigations on the electronic structure of Mn$_{12}$-th and Mn$_{12}$-biph.

The photoelectron intensity which is proportional to the Mn $3d$ PDOS of the Mn$_{12}$ monolayers was obtained by subtracting the off-resonance (labeled O) spectra from the on-resonance (labeled *B*, *C*, and *D*) ones. Figure 7 shows the corresponding intensity obtained from RPES difference spectra. The strongest on-resonance RPES curve (energy labeled *A* in Figs. 5 and 6) must not be used for extraction of the contribution of intact Mn$_{12}$ clusters to the Mn $3d$ PDOS since it is attributed to Mn^{2+}. Even the *B-O* difference spectra exhibit a significant Mn^{2+} contribution. The *C-O* difference spectrum still includes a contribution from the molecular fragments that give rise to the Mn^{2+} signal and is thus not further considered. Solely the *D-O* difference spectra can be attributed to purely Mn^{3+} and Mn^{4+} contributions. For these spectra, the Mn $3d$ DOS of Mn$_{12}$ as previously calculated by LDA+U for $U=4$ eV (Refs. 16 and 28) is reproduced. The

PDOS is spread uniformly over a range of about 10 eV while a band gap sets in about 1 eV below the Fermi level, supporting the insulating nature of Mn_{12} clusters. The line shape of the Mn_{12}-th *D-O* difference spectrum coincides with the theoretical Mn 3*d* DOS reported in Ref. [28] except for an energy shift of about 2 eV while the line shape of Mn_{12}-biph is closer to that reported in Ref. [16]. An energy shift between calculated and measured spectra might be attributed to the interaction between Mn_{12} molecules and the 4-MTBA functionalization layer. Preliminary STM and STS results reproduce the position of the band gap edge below E_F measured by RPES.[30] The difference between Mn_{12}-th and Mn_{12}-biph *D-O* difference spectra could be explained by the respective ligands, inducing slightly different Mn_{12}-core symmetries. Small contributions from molecular fragments containing Mn^{3+} or Mn^{4+} could also slightly change the spectral line shape while the contribution from the fragments alone would presumably not reproduce the previous LDA+U calculations. These facts indicate the presence of a finite number of intact Mn_{12} cores and support the importance of taking into account electron correlation for theoretical calculations on Mn_{12} clusters. We conclude that the clusters observed in STM images of Mn_{12}-th and Mn_{12}-biph on 4-MTBA functionalized Au (Fig. 2) are intact Mn_{12}-molecules accompanied by some fraction of Mn^{2+} containing fragments.

IV. CONCLUSIONS

Monolayers of Mn_{12}-th chemically grafted on clean as well as on functionalized Au surfaces and monolayers of Mn_{12}-biph grafted on functionalized Au surfaces have been studied by means of STM, XPS, XAS, and RPES. STM and XPS were employed to investigate the monolayer deposition. Formation of Mn_{12} monolayers was observed in the case of Mn_{12}-th and Mn_{12}-biph on 4-MTBA. Direct deposition of Mn_{12}-th onto the Au surface leads to a strong fragmentation of Mn_{12} cores. By using XAS and RPES performed at the Mn 2*p*-3*d* absorption edge we investigated the electronic structure of deposited Mn_{12} clusters. XAS measurements reveal a significant deviation of the spectral line shapes obtained from SMM monolayers from those obtained from SMM single crystals. However, a large amount of Mn_{12} cores seems to retain their structural integrity upon surface deposition by using an appropriate combination of Mn_{12} cluster and substrate functionalization. By extracting the Mn 3*d* partial density of states from the RPES spectra of Mn_{12}-th and Mn_{12}-biph on 4-MTBA/Au a very good agreement with previously reported LDA+U calculations for U=4 eV was found, showing the importance of electron correlation effects in Mn_{12} systems.

*Electronic address: soenke.voss@uni-konstanz.de

[1] R. Sessoli, D. Gatteschi, A. Caneschi, and M. A. Novak, Nature (London) **365**, 141 (1993).

[2] M. N. Leuenberger and D. Loss, Nature (London) **410**, 789 (2001).

[3] T. Lis, Acta Crystallogr., Sect. B: Struct. Crystallogr. Cryst. Chem. **36**, 2042 (1980).

[4] A. Caneschi, D. Gatteschi, R. Sessoli, A. L. Barra, L. C. Brunel, and M. Guillot, J. Am. Chem. Soc. **113**, 5873 (1991).

[5] L. Thomas, F. Lionti, R. Ballou, D. Gatteschi, R. Sessoli, and B. Barbara, Nature (London) **383**, 145 (1996).

[6] W. Wernsdorfer, M. Murugesu, and G. Christou, Phys. Rev. Lett. **96**, 057208 (2006).

[7] A. Naitabdi, J.-P. Bucher, P. Gerbier, P. Rabu, and M. Drillon, Adv. Mater. (Weinheim, Ger.) **17**, 1612 (2005).

[8] H. B. Heersche, Z. de Groot, J. A. Folk, H. S. J. van der Zant, C. Romeike, M. R. Wegewijs, L. Zobbi, D. Barreca, E. Tondello, and A. Cornia, Phys. Rev. Lett. **96**, 206801 (2006).

[9] M.-H. Jo, J. Grose, K. Baheti, M. M. Deshmukh, J. J. Sokol, E. M. Rumberger, D. N. Hendrickson, J. R. Long, H. Park, and D. C. Ralph, Nano Lett. **6**, 2014 (2006).

[10] M. Mannini, D. Bonacchi, L. Zobbi, F. M. Piras, E. A. Speets, A. Caneschi, A. Cornia, A. Magnani, B. J. Ravoo, D. N. Reinhoudt, R. Sessoli, and D. Gatteschi, Nano Lett. **5**, 1435 (2005).

[11] A. Cornia, A. C. Fabretti, M. Pacchioni, L. Zobbi, D. Bonacchi, A. Caneschi, D. Gatteschi, R. Biagi, U. D. Pennino, V. D. Renzi, L. Gurevich, and H. S. J. van der Zant, Angew. Chem. **115**, 1683 (2003).

[12] L. Zobbi, M. Mannini, M. Pacchioni, G. Chastanet, D. Bonacchi, C. Zanardi, R. Biagi, U. D. Pennino, D. Gatteschi, A. Cornia, and R. Sessoli, Chem. Commun. (Cambridge) **2005**, 1640.

[13] E. Coronado, A. Forment-Aliaga, F. M. Romero, V. Corradini, R. Biagi, V. D. Renzi, A. Gambardella, and U. D. Pennino, Inorg. Chem. **44**, 7693 (2005).

[14] B. Fleury, L. Catala, V. Huc, C. David, W. Z. Zhong, P. Jegou, L. Baraton, S. Palacin, P.-A. Albouy, and T. Mallah, Chem. Commun. (Cambridge) **2005**, 2020.

[15] G. G. Condorelli, A. Motta, M. Fevazza, P. Nativo, I. L. Fragala, and D. Gatteschi, Chem.-Eur. J. **12**, 3558 (2006).

[16] U. D. Pennino, V. D. Renzi, R. Biagi, V. Corradini, L. Zobbi, A. Cornia, D. Gatteschi, F. Bondino, E. Magnano, M. Zangrando, M. Zacchigna, A. Lichtenstein, and D. W. Boukhvalov, Surf. Sci. **600**, 4185 (2006).

[17] J. M. Lim, Y. Do, and J. Kim, Eur. J. Inorg. Chem. **2006**, 711.

[18] D. Ruiz-Molina, P. Gerbier, E. Rumberger, D. B. Amabilino, I. A. Guzei, K. Folting, J. Huffman, A. Rheingold, G. Christou, J. Veciana, and D. N. Hendrickson, J. Mater. Chem. **12**, 1152 (2002).

[19] M. Aguilar, E. Anguiano, J. A. Aznárez, and J. L. Sacedón, Surf. Sci. **482-485**, 935 (2001).

[20] P. Artus, C. Boskovic, J. Yoo, W. E. Streib, L.-C. Brunel, D. N. Hendrickson, and G. Christou, Inorg. Chem. **40**, 4199 (2001).

[21] P. Cyganik, M. Buck, W. Azzam, and C. Wöll, J. Phys. Chem. B **108**, 4989 (2004).

[22] S. Phark, Z. G. Khim, B. J. Kim, B. J. Suh, S. Yoon, J. Kim, J. M. Lim, and Y. Do, Jpn. J. Appl. Phys., Part 1 **43**, 8273 (2004).

[23] B. J. Kim, B. J. Suh, S. Yoon, S. H. Phark, Z. G. Khim, J. Kim, J. M. Lim, and Y. Do, J. Korean Phys. Soc. **45**, 1593 (2004).

[24] A. Naitabdi, J. P. Bucher, P. Rabu, O. Toulemonde, and M. Drillon, J. Appl. Phys. **95**, 7345 (2004).

[25] J.-S. Kang, J. H. Kim, Y. J. Kim, W. S. Jeon, D.-Y. Jung, S. W. Han, K. H. Kim, K. J. Kim, and B. S. Kim, J. Korean Phys. Soc. **40**, L402 (2002).

[26] P. Ghigna, A. Campana, A. Lascialfari, A. Caneschi, D. Gatteschi, A. Tagliaferri, and F. Borgatti, Phys. Rev. B **64**, 132413 (2001).

[27] R. Moroni, C. Cartier dit Moulin, G. Champion, M.-A. Arrio, P. Sainctavit, M. Verdaguer, and D. Gatteschi, Phys. Rev. B **68**, 064407 (2003).

[28] D. W. Boukhvalov, E. Z. Kurmaev, A. Moewes, M. V. Yablonskikh, S. Chiuzbaian, V. R. Galakhov, L. D. Finkelstein, M. Neumann, M. I. Katsnelson, V. V. Dobrovitski, and A. L. Lichtenstein, J. Electron Spectrosc. Relat. Phenom. **137-140**, 735 (2004).

[29] L. F. Mattheiss and R. E. Dietz, Phys. Rev. B **22**, 1663 (1980).

[30] S. Voss and M. Fonin (unpublished).